Received: Added at production | Revised: Added at production | Accepted: Added at production

DOI: xxx/xxxx

ARTICLE TYPE

Hierarchical robust control for variable-pitch wind turbine with actuator faults

Sina Ameli[1] | Olugbenga Moses Anubi[2]

[1]Electrical Engineering Department, Center for Advanced Power Systems (CAPS), Florida State University, Florida, USA
[2]Electrical Engineering Department, Center for Advanced Power Systems(CAPS), Florida State University, Florida, USA

Correspondence
*Olugbenga Moses Anubi, Electrical Engineering Department, Center for Advanced Power Systems (CAPS), Florida State University, Tallahassee, Florida, 32310, USA. Email: oanubi@fsu.edu

Summary

In this brief, we develop a fault tolerant control (FTC) using a hierarchical-robust methodology with guaranteed stability for a wind turbine (WT), which is subject to an exogenous input, and an actuator fault. The high-level control is designed to robustly compensate for the nonlinearities, uncertainty, and disturbance in the system. The low-level control is designed to robustly automatically allocate control authority among redundant actuators mitigating an actuator fault. At the low-level, the robust control problem is transformed into an equivalent optimal control problem. Finally, the developed FTC is validated using a comprehensive simulation study on a 5MW variable-pitch wind turbine model given in the Fatigue, Aerodynamics, Structures, and Turbulence (FAST) simulator provided by the U.S. National Renewable Energy Laboratory (NREL). The results show that the developed FTC retains robust performance in the presence of wind disturbance, and a time-varying actuator fault.

KEYWORDS:
Robust control, γ-dissipativity, optimal control, fault tolerant control, variable-pitch wind turbine

1 | INTRODUCTION

It is well-known that wind is becoming an increasingly significant form to meet future energy requirements [1,2,3,4,5]. However, its market penetration has been adversely affected due to high maintenance costs for MW-scale wind turbines (WTs). To expand the lifetime of such large modern WTs, using active load alleviation control is critical [6,7]. One effective approach to decrease structural loading, thereby extending the lifetime of the WTs' components, while generating the rated electrical power is to use pitch control [8,9,10,11]. A variety of pitch control strategies have been proposed in literature [12,13]. In [12], and [14] a Proportional-Integral controller for the blade pitch angle is designed to decrease the mechanical stress. However, the design is highly dependent on the wind speed – which imposes additional constrain/cost of instrumenting for accurate wind speed measurement. In [15] a linear quadratic regulator for pitch control is proposed. Although the simulation results show a precise tracking of the generator speed, they are only shown for a limited range of wind speed. Likewise, linear quadratic Gaussian control [13,16] cannot properly work at different operating points.

In order to mitigate the effect of model variation, a variety of nonlinear controllers have been proposed for WTs. In [17] a gain-scheduled-optimal controller is proposed which uses genetic algorithm for pitch control. However, it requires the knowledge of the WT's dynamics at different operating points. The authors in [18] use a Fuzzy logic based approach which, though shows significant promise for nonlinear system, has too many non-intuitive parameters to be tuned. A linear parameter varying (LPV) controller is developed in [19] but it requires exact dynamic model at different operating points. An $\boldsymbol{l}_1$ optimal controller, which is based on gain-scheduling approach, is developed in [20] for the pitch control of a 5MW WT using its linear model at different

operating points but, due to the interpolation operation, the overall performance of the controller is degraded when the system switches from one operating point to the other. In[21], the authors implement a feedback linearization scheme; however, this method requires accurate modeling of the WT. An SMC is proposed for a DFIG-based WT in[22]. An adaptive SMC is developed in[23]; however, the results show considerable chattering which could be harmful for the actuators. An adaptive integral sliding mode control (SMC) is developed in[24].While satisfactory performance is achieved, the results show that the closed-loop system suffers from peaking phenomena.

Moreover, it is inevitable that a WT encounters internal fault(s) at some points during its useful life and operation. This can happen in sensors, actuators and/or other significant components of the system[25,26,27,28]. In particular, several types of faults could occur in pitch actuators. Pitch actuator faults can happen due to hydraulic leakage, high-air content, and pump wear changing its dynamics[25,28] or an offset in the pitch actuator[29]. The pitch systems collaboratively control the speed of the WT when the wind speed is above the rated value (full-load region). When there is no fault and each pitch system is operating efficiently as designed, the total control authority is divided equally among them. Thus, baseline control are usually designed with only one pitch dynamic with small parametric variations handled by inherent robustness of the control system. However, when there is fault in any of the pitch subsystems, the faulty actuator can no longer deliver on the reference commands. Depending on the fault scenario, if the underlying low-level controller is sufficiently robust, it may readjust to achieve good tracking. However, when this happens, there is unnecessary loss of efficiency as the robust control requires higher control authority in terms of either higher gain, frequency or both. On the other hand, if the underlying low-level control is not sufficiently robust, or at least adaptive to the fault, the overall system suffers from the deficiency. Thus, there is a need for collaborative management of the faulty situation, where the healthy actuators efficiently take up the deficiencies in the faulty ones in order to achieve overall system objectives while not loosing much on overall efficiency.

Consequently, fault tolerant control (FTC) plays a pivotal role in WT technology. Two kinds of FTC have appeared in literature; Passive Fault Tolerant Control (PFTC),[30,31,32,23,33,34] and Active Fault Tolerant Control (AFTC)[35,36,37,38,29,39,40,41,42,43]. PFTC is a robust control designed to stabilize the system and also meet the required performance of the system under the faulty system. AFTC, however, uses detection and diagnoses techniques along with the controller. While the PFTC does not use any fault detection method, its structure, design, and implementation is much simpler than AFTC. A virtual sensor and actuator (VSA), Takagi-Sugeno (TS) fuzzy based, and an adaptive FTC[44] approaches have been proposed for a WT in the full-load region. However, in almost all the cases, there is considerable negative spikes in the electrical power signal when fault occurs in the pitch actuators.

In order to leverage the simplicity of PFTC, while achieving the robustness of AFTC, this paper considers a layered-structure control development approach. The developed hierarchical robust control is shown in Fig. 1. The high-level control loop is designed to compensate for wind disturbance, model uncertainty, and nonlinearity. The low-level control is designed to allocate the aggregated command from the high-level while mitigating with pitch actuator faults. This is done via a *splitter* design. In general, the splitter implements the solution to an optimization problem which formulated to incorporate relevant multi-objective performance and operational constraints. The main contributions pursued in this paper are:

1. Reformulating the rotor dynamics to incorporate a more realistic nonlinear phenomenological model of the control effectiveness. This exposes the dependence on a vector of pitch angles and contrary to existing approaches,[15,24,45,46], which only rely on the linearized effectiveness with respect to the pitch angle.

2. A high-level robust control structure for compensating for nonlinearities, uncertainties and unmeasurable wind speed in the control input effectiveness. Existing approaches[20,47,48,49] either suppose that the wind speed is measurable in their design for simplicity, or the controller design relies on a wind speed observer which either attempts to estimate the wind speed directly[9,16,50,51,52,53,54], or the power coefficient which itself depends on the wind speed[29,55]. In any case, it is extremely difficult to accurately estimate those quantities, thereby resulting in overall closed-loop performance degradation.

3. A low-level design which involves converting a robust control problem into an equivalent optimal control problem. The equivalent optimal control problem is easily solvable using LQR-like development, and is shown to be a solution to the robust control problem which is formulated to mitigate actuator faults. Simulation results show that the resulting generator power is much smoother, with negative spikes eliminated.

4. Rigorous stability analysis for each layer of the developed fault tolerant control.

The rest of the paper is organized as follows: Section 2 introduces the notations and convention employed throughout the paper. Section 3 develops the system model, including the derive-train dynamics, pitch actuator dynamics and the fault model.

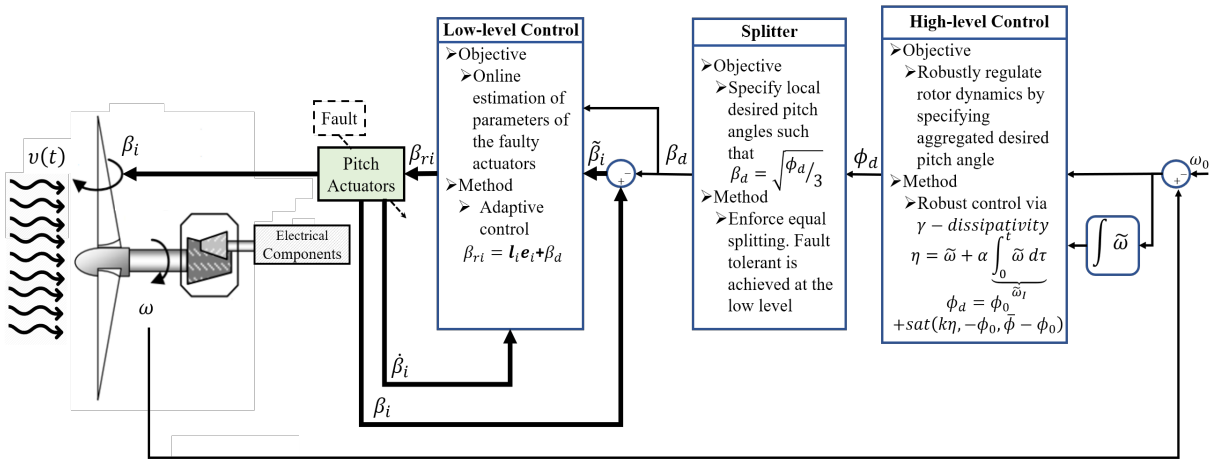

FIGURE 1 Hierarchical layers of the proposed controller

Section 4 presents the control development for all layers. Section 5, presents the numerical simulation results. Finally, concluding remarks are given in Sections 6.

2 | NOTATION AND PRELIMINARY

The following notions and conventions are employed throughout the paper: $\mathbb{R}$,$\mathbb{R}^n$,$\mathbb{R}^{n\times m}$ denote the space of real numbers, real vectors of length n and real matrices of n rows and m columns, respectively. $\mathbb{R}_+$ denotes positive real numbers. $X^\top$ denotes the transpose of the quantity X. Normal-face lower-case letters ($x \in \mathbb{R}$) are used to represent real scalars, bold-face lower-case letter ($\mathbf{x} \in \mathbb{R}^n$) represents vectors, while normal-face upper case ($X \in \mathbb{R}^{n\times m}$) represents matrices. The euclidean balls $\mathbb{B}_r(0)$ and $\mathbb{B}_r(\mathbf{x}_0)$ are defined respectively for some $r \in \mathbb{R}_+$ as $\mathbb{B}_r(0) \triangleq \{\mathbf{x} : \|\mathbf{x}\| \leq r\}$ and $\mathbb{B}_r(\mathbf{x}_0) \triangleq \{\mathbf{x} : \|\mathbf{x} - \mathbf{x}_0\| \leq r\}$. The space of all square-integrable signals defined as

$$\mathcal{L}_2^n \triangleq \left\{ \mathbf{f} : \mathbb{R}_+ \mapsto \mathbb{R}^n \;\middle|\; \int_0^\infty \|f(\tau)\|^2 \, d\tau < \infty \right\}.$$

For each $T \in \mathbb{R}_+$, the function $\mathbf{f}_T : \mathbb{R}_+ \mapsto \mathbb{R}^n$ is defined by

$$\mathbf{f}_T(t) \triangleq \begin{cases} \mathbf{f}(t), & 0 \leq t < T \\ \mathbf{0}, & t \geq T \end{cases},$$

and is called the *truncation* of $\mathbf{f}$ to the interval $[0, \ T]$. Consequently, the set $\mathcal{L}_{2e}^n$ of all measurable signal $\mathbf{f} : \mathbb{R}_+ \mapsto \mathbb{R}^n$ such that $\mathbf{f}_T(t) \in \mathcal{L}_2$ for all $T \in [0, \ \infty)$ is called the extension of $\mathcal{L}_2^n$ or the extended $\mathcal{L}_2$-space.

Definition 1. (Finite-Gain $\mathcal{L}$-stability) Consider the nonlinear system

$$\mathcal{H} : \quad \begin{aligned} \dot{\mathbf{x}} &= f(\mathbf{x}, \mathbf{v}) \\ \mathbf{z} &= h(\mathbf{x}) \end{aligned} \tag{1}$$

where $\mathbf{x} \in \mathcal{L}_{2e}^n$, $\mathbf{v} \in \mathcal{L}_{2e}^p$, $\mathbf{z} \in \mathcal{L}_{2e}^m$ are the state, input, and output vector signals, respectively. The system in (1), considered as a mapping of the form $\mathcal{H} : \mathcal{L}_{2e}^p \mapsto \mathcal{L}_{2e}^m$ is said to be finite-gain $\mathcal{L}_2$-stable if there exists real non-negative constants γ, β such that $\|\mathcal{H}(\mathbf{v})\|_2 \leq \gamma \|\mathbf{v}\|_2 + \beta$. Moreover, $\gamma^* = \inf \{\gamma \ : \ \|\mathcal{H}(\mathbf{v})\|_2 \leq \gamma \|\mathbf{v}\|_2 + \beta\}$ is the corresponding $\mathcal{L}_2$-gain (will be referred to as gain) of the system.

Definition 2. (γ-dissipativity) The dynamic system (1) is dissipative with respect to the supply rate $s(\mathbf{v}, \mathbf{z}) \in \mathbb{R}$, if there exists an energy function $V(\mathbf{x}) \geq 0$ such that, for all $t_f \geq t_0$,

$$V(\mathbf{x}(\mathbf{t_f})) \leq V(\mathbf{x}(\mathbf{t_0})) + \int_{t_0}^{t_f} s(\mathbf{v}, \mathbf{z}) dt \quad \forall \quad \mathbf{v} \in \mathcal{L}_{2e}. \tag{2}$$

Moreover, given a positive scalar γ, if the supply rate is taken as $s(\mathbf{v}, \mathbf{z}) = \gamma^2 \|\mathbf{v}\|_2^2 - \|\mathbf{z}\|_2^2$, then the dissipation inequality in (2) implies a finite-gain $\mathcal{L}_2$ stability[56]. Consequently, the system is said to be γ-dissipative and the dissipativity inequality in (2) becomes

$$\dot{V} \leq \gamma^2 \|\mathbf{v}\|_2^2 - \|\mathbf{z}\|_2^2$$

Definition 3. (sat) Given two real numbers $x_1 \leq 0 \leq x_2$, a function $\mathsf{sat} : \mathbb{R}^n \mapsto \mathbb{R}^n$ is defined element-wise as:

$$\mathsf{sat}(\mathbf{x}, x_1, x_2)_i \triangleq \begin{cases} x_2 & \text{if } x_i \geq x_2 \\ x_i & \text{if } x_1 \leq x_i \leq x_2 \\ x_1 & \text{otherwise} \end{cases}. \tag{3}$$

Lemma 1. The following properties hold[57]

1. $\mathsf{sat}(\alpha \mathbf{x}, x_1, x_2) = \alpha \mathsf{sat}(\mathbf{x}, \frac{x_1}{\alpha}, \frac{x_2}{\alpha})$, for all $\alpha > 0$
2. Given $r > 0$, there exists $\alpha_r > 0$ such that $\mathbf{x}^\top \mathsf{sat}(\mathbf{x}, x_1, x_2) \geq \alpha_r \|\mathbf{x}\|^2$, for all $\mathbf{x} \in \mathbb{B}_r(0)$

Proof. the first statement is straightforward from the definition. The second statement holds by setting

$$\alpha_r = \begin{cases} 1 & \text{if } r \leq x_m \\ \frac{x_m}{r^2}\left(2r - x_m\right) & \text{if } r \geq x_m \end{cases},$$

where $x_m = \min\{|x_1|, |x_2|\}$. □

3 | SYSTEM MODEL DEVELOPMENT

WTs generally operate in two regions shown in Figure 2. In the partial-load region, the WT can produce an optimum amount of power. This is usually achieved by some form of torque control. In the full-load region, the wind speed is above the rated value; as a result, the rated electrical power can be generated while reducing the mechanical stress using the pitch control.

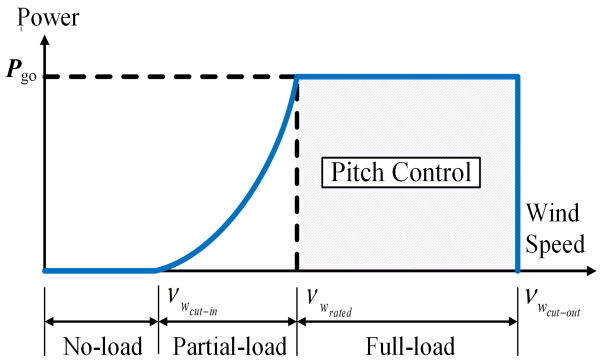

FIGURE 2 Ideal power curve versus wind speed for the operation of a typical WT[24]

Figure 3 shows a schematic of a typical WT with the different control systems covering both the partial-load and the full-load regions. Next, in order to facilitate the subsequent control design, an outline of the dynamical model for the relevant subsystems of the WT is given.

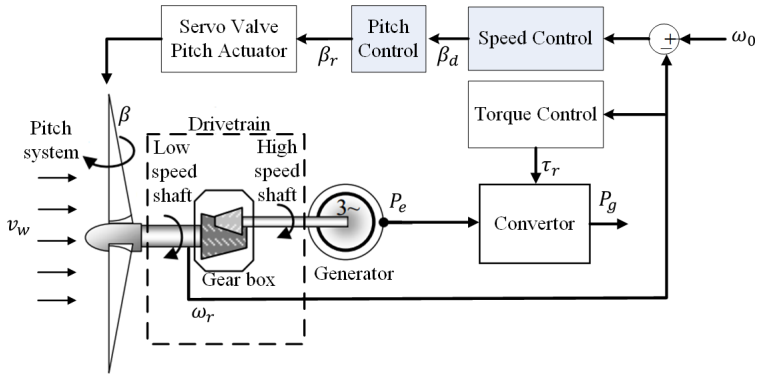

FIGURE 3 Overall schematic diagram of a WT control system[24]

3.1 | Drive-train Dynamics

A lumped-parameter model of the rotor–generator sub-assembly is given by[58,59]

$$\dot{\omega} = b_1(v, \omega) - b_2(v, \omega)||\boldsymbol{\beta}||^2 \tag{4}$$

where $\omega \in \mathbb{R}$ is the rotor speed, $\boldsymbol{\beta} \in \mathbb{R}^3$ is a vector of the pitch angle, $v \in \mathbb{R}_+$ is the wind speed, and

$$b_1(v, \omega) = \frac{cv^3}{2J\omega}\left(\frac{v}{\omega} - m_1\right)\mathrm{e}^{(-m_2\frac{v}{\omega})} - \frac{P_0}{J\omega}$$
$$b_2(v, \omega) = \frac{cv^3}{6J\omega}m_3\mathrm{e}^{(-m_2\frac{v}{\omega})}$$

are obtained from a phenomenological model of the aerodynamic torque[60] with experimentally determined positive constants m_1, m_2, m_3, c, and P_0 is the rated mechanical power, J is the total drive-train inertia. As given by (4), the rotor dynamics is driven by an aggregation of the pitch angles. This drives the motivation for the hierarchical control where the high level specifies the desired aggregation and low levels, in turns, specify local pitch angles such that the specified aggregation is achieved, while mitigating any fault in the local subsystem.

3.2 | Pitch actuator dynamics

Each independently controlled pitch system comprises of hydraulic piston servo mechanism whose responses are typically abstracted by the second order characteristic model

$$\beta_i = \frac{\omega_{n_i}^2}{s^2 + 2\zeta_i\omega_{n_i}s + \omega_{n_i}^2}\beta_{ri}, \qquad i = 1, 2, 3, \tag{5}$$

where ζ_i, and ω_{n_i} are the damping ratios and natural frequencies of actuators, respectively. β_i, and β_{ri} are the corresponding pitch angle outputs and the reference pitch inputs for each system, respectively.

3.2.1 | Fault Model

One fault could occur in pitch actuators is due to the high-air content, which causes air-oil mixture. Moreover, it is well known that when such a fault occurs, it alters the natural frequency and damping ratio[61]. Thus, the uncertainty caused by this fault is

considered parametric and can be modeled as

$$\omega_n^2 = \omega_{n_0}^2 (1+\delta), \qquad (6)$$
$$\zeta\omega_n = \zeta_0\omega_{n0}(1+\rho),$$

where ω_{n_0} and ζ_0 are the respective natural frequency and the damping ratio at the operation point (free-fault situation). Moreover, δ and ρ are uncertain parameters but bounded as $-1 < -\underline{\delta} \leq \delta \leq 0$, $-1 < -\underline{\rho} \leq \rho \leq 0$ for some known positive constants $\underline{\delta}$ and $\underline{\rho}$. Consequently, the uncertainty model above can be written as

$$\omega_n^2 = \omega_{n_0}^2 \left(\hat{\delta} + \Delta_\delta\right), \qquad (7)$$
$$\zeta\omega_n = \zeta_0\omega_{n0}\left(\hat{\rho} + \Delta_\rho\right),$$

where Δ_δ and Δ_ρ are positive quantities upper bounded by 1, $\hat{\rho} \triangleq 1 - \underline{\rho}$ and $\hat{\delta} \triangleq 1 - \underline{\delta}$.

4 | CONTROL DEVELOPMENT

The control design is done in three stages. First, a high-level controller is designed to make the $\mathcal{L}_2$-gain from the wind speed variation to rotor speed variation as small as possible. Second, a splitter distributes the desired pitch signal to the low-level control loop. Finally, a robust low-level control law is designed to then track the allocated pitch desired signals from the high-level control.

4.1 | Drive-train control

The objective of this control design is to robustly regulate the rotor speed against wind speed variation. This is done using the γ-dissipativity described in the preliminary section. The control signal for this purpose is the aggregated pitch angle $\|\boldsymbol{\beta}\|^2$ corresponding to the aerodynamic torque. Throughout this subsection, in order to facilitate clear exposition, the substitution $\phi \triangleq \|\boldsymbol{\beta}\|^2$ is used for the rotor dynamics in (4). In addition, the following assumptions are made concerning the model:

Assumption 1. There exists a positive constant c_b such that

$$c_b < b_2(v,\omega) \quad \text{for all } \omega \in \mathbb{R}, v \in \mathbb{R}_+$$

This is a reasonable assumption for the full-load region, as depicted in Figure 2, since the rotor and wind speeds are both lower and upper bounded by constants.

Assumption 2 (Bounded disturbance input effectiveness)**.** There exists a positive constant c_v such that

$$\left|\frac{\partial}{\partial v}\left(b_1(v,\omega) - b_2(v,\omega)\phi_0\right)\right| \leq c_v,$$

for all v.

Consequently, the rotor tracking error is given by

$$\widetilde{\omega} = \omega - \omega_0,$$

Consider the filtered tracking error

$$\eta = \widetilde{\omega} + \alpha \underbrace{\int_0^t \widetilde{\omega}(\tau)d\tau}_{\widetilde{\omega}_I},$$

where α is a positive constant. Taking first time derivative yields

$$\begin{aligned}\dot{\eta} =&\dot{\widetilde{\omega}} + \alpha\widetilde{\omega}\\ =&\dot{\omega} + \alpha\widetilde{\omega}\\ =&b_1(v,\omega) - b_2(v,\omega)\phi + \alpha\widetilde{\omega}\end{aligned}$$

Substituting the rotor dynamics in (4), and adding and subtracting the terms $b_1(v_0,\omega)$, $b_2(v,\omega)\phi_0$, and $b_2(v_0,\omega)\phi_0$, yields

$$\dot{\eta} = \underbrace{\left(b_1(v,\omega) - b_2(v,\omega)\phi_0\right)}_{f(v,\omega)} - \underbrace{\left(b_1(v_0,\omega) - b_2(v_0,\omega)\phi_0\right)}_{f(v_0,\omega)} + \underbrace{b_1(v_0,\omega) - b_2(v_0,\omega)\phi_0}_{\psi_0} - b_2(v,\omega)\underbrace{(\phi - \phi_0)}_{\widetilde{\phi}} + \alpha\widetilde{\omega}, \tag{8}$$

which after using the Mean Value Theorem [62] yields

$$\dot{\eta} = \psi_0 + \alpha\widetilde{\omega} - b_2(v,\omega)\widetilde{\phi} + L_v\widetilde{v}, \tag{9}$$

where

$$\begin{aligned}f(v,\omega) - f(v_0,\omega) =&\left.\frac{\partial f(v,\omega)}{\partial v}\right|_{v=\varepsilon v_0+(1-\varepsilon)v}\underbrace{(v - v_0)}_{\tilde{v}}, \quad \text{for some } \varepsilon \in [0\ \ 1]\\ =&\underbrace{\left(\frac{\partial}{\partial v}\left(b_1(v,\omega) - b_2(v,\omega)\phi_0\right)\right)}_{L_v}\Bigg|_{v=\varepsilon v_0+(1-\varepsilon)v}\tilde{v}\end{aligned}$$

Assumption 3 (Nominal Stability)**.** Since at rated conditions, the WT, together with other systems downstream, have enough damping such that the system is nominally asymptotically stable. For that reason, it is assumed that

$$\eta\psi_0 \le 0$$

Consequently, the control law is designed as

$$\phi = \phi_0 + \mathsf{sat}\left(k\eta, -\phi_0, \bar{\phi} - \phi_0\right), \tag{10}$$

where $\bar{\phi}$ is the maximum allowed aggregated pitch angle, and k is a positive constant.

The achieved closed-loop performance is summarized in the main result bellow.

Theorem 1 (Main Result)**.** Consider the control law in (10) where the control gains k, and α are chosen to satisfy the sufficient condition

$$k - \frac{(1+\alpha)}{c_b\alpha_r} \ge \frac{c_v^2}{4\gamma^2 c_b\alpha_r} \tag{11}$$

for some real number $\gamma > 0$. Suppose that there exists a positive constant $\bar{\sigma_v} > 0$ such that the wind disturbance is bounded as $|\tilde{v}| \le \bar{\sigma_v}$. Then, if the initial condition satisfies the inclusion

$$\eta(0) \in \mathbb{B}_r(0) \tag{12}$$

with $r \triangleq \gamma\bar{\sigma_v}$, the closed-loop error system in (9), is $\gamma - dissipative$.

Proof. Consider the energy function

$$V = \frac{1}{2}\eta^2 + \frac{\alpha^2}{2}\widetilde{\omega}_I^2$$

taking first time derivative yields

$$\begin{aligned}\dot{V} &= \eta\dot{\eta} + \alpha^2\widetilde{\omega}_I\widetilde{\omega}\\ &= \eta\left(\psi_0 + \alpha\left(\eta - \alpha\widetilde{\omega}_I\right) - b_2\mathsf{sat}\left(k\eta, -\phi_0, \bar{\phi} - \phi_0\right) + L_v\widetilde{v}\right) + \alpha^2\widetilde{\omega}_I\left(\eta - \alpha\widetilde{\omega}_I\right)\\ &= \eta\psi_0 + \alpha\eta^2 - \frac{1}{k}b_2(v,\omega)\,(k\eta)\,\mathsf{sat}\left(k\eta, -\phi_0, \bar{\phi} - \phi_0\right) + \eta L_v\widetilde{v} - \alpha^3\widetilde{\omega}_I^2\end{aligned}$$

Adding and subtracting $\left(\gamma^2\widetilde{v}^2 - \eta^2\right)$, and using Assumption. 1, and Assumption. 3 yields

$$\begin{aligned}\dot{V} &\leq \alpha\eta^2 - \frac{c_b}{k}(k\eta)\,\mathsf{sat}\left(k\eta, -\phi_0, \bar{\phi}-\phi_0\right) + \eta L_v\widetilde{v} + \gamma^2\widetilde{v}^2 - \eta^2 + \eta^2 - \gamma^2\widetilde{v}^2 - \alpha^3\widetilde{\omega}_I^2 \\ &\leq (\alpha+1)\,\eta^2 - \frac{c_b}{k}(k\eta)\,\mathsf{sat}\left(k\eta, -\phi_0, \bar{\phi}-\phi_0\right) - \gamma^2\left(\widetilde{v} - \frac{L_v}{2\gamma^2}\eta\right)^2 + \frac{L_v^2}{4\gamma^2}\eta^2 - \alpha^3\widetilde{\omega}_I^2 + \gamma^2\widetilde{v}^2 - \eta^2 \\ &\leq \left(\alpha + 1 + \frac{L_v^2}{4\gamma^2}\right)\eta^2 - \frac{c_b}{k}(k\eta)\,\mathsf{sat}\left(k\eta, -\phi_0, \bar{\phi}-\phi_0\right) - \alpha^3\widetilde{\omega}_I^2 + \gamma^2\widetilde{v}^2 - \eta^2\end{aligned}$$

Using Lemma 1, and Asssumption 2 leads to

$$\dot{V} \leq \left(\alpha + 1 + \frac{c_v^2}{4\gamma^2} - c_b k\alpha_r\right)\eta^2 + \gamma^2\widetilde{v}^2 - \eta^2 \quad \text{for all} \;\; \eta \in \mathbb{B}_r(0)$$

Applying the sufficient condition (11) leads to

$$\dot{V} \leq \gamma^2\widetilde{v}^2 - \eta^2, \quad \text{for all} \;\; \eta \in \mathbb{B}_r(0) \tag{13}$$

Now, since $\widetilde{v}^2 < \bar{\sigma_v}^2$, then $\dot{V} < 0$ whenever $\eta > r$. Thus, $\eta(0) < r$ implies that the set $\mathbb{B}_r(0)$ is positively invariant and (13) holds with the set. Thus, the conclusion holds given the sufficient condition in (11) and the initial condition inclusion in (12). □

Remark 1. $\gamma - dissipative$ implies that $\|\eta(s)\|_2 \leq \gamma\left\|\widetilde{v}\right\|_2$ which also implies that

$$\left\|\left(1 + \frac{\alpha}{s}\right)\widetilde{\omega}(s)\right\|_2 \leq \gamma\left\|\widetilde{v}(s)\right\|_2.$$

Now, since $\left\|\widetilde{\omega}(s)\right\|_2 \leq \left\|\left(1 + \frac{\alpha}{s}\right)\widetilde{\omega}(s)\right\|_2$, it follows that

$$\left\|\widetilde{\omega}(s)\right\|_2 \leq \gamma\left\|\widetilde{v}(s)\right\|_2.$$

Thus, (9) seen as the mapping $\widetilde{v} \mapsto \widetilde{\omega}$ is also $\gamma - dissipative$ for all $\alpha > 0$.

4.2 | Spliter design

As shown in Fig. 1, the objective of the splitter is to translate the hierarchical desired aggregated pitch angle to individual desired pitch angle for the low-level control. Since the fault scenario considered in this paper is transient fault, (as against permanent actuator damage), the fault-tolerant problem is deferred to the low-level controller and the splitting problem is defined to enforce equal splitting among each desired pitch angle. This is consistent with existing approaches in literature[23,63,64]. However, this structure allows us to incorporate multiple fault scenarios, including a combination of transient faults and permanent actuator damage in which any permanently damaged actuator needs to be taken offline completely, while resiliently specifying tracking for the other actuators. This particular splitting problem is challenging because it introduces additional switching dynamics whose effect needs to be taking into account from both the high-level control to the low-level control problem. Due to space limitation, and not to divert too much from the original scope of the current paper, we will focus more on the elaborate splitter design in future work. For the time being, assuming equal splitting for each desired pitch angle, the splitter algorithm is given by:

$$\beta_d = \sqrt{\frac{\phi_d}{3}}$$

4.3 | Pitch control

In this section, the control development is carried out for a single actuator. The resulting control structure is then applied for all the actuators. This does not result in any loss of generality since the model structure given in (5) is the same for all actuators. Let $\tilde{\beta} = \beta - \beta_d$ be the corresponding tracking error. Since the pitch actuators are much faster than the rotor dynamics, it is reasonable to assume that $\dot{\beta}_d = 0$ for the pitch control development. Alternatively, one could use singular perturbation to separate the dynamic into slow-and fast-time scales, with the fast-time scale dynamic decaying exponentially fast depending on the perturbation parameter. The controller development is then done to stabilize the slow-time scale dynamic[65,66].

In the end, the resulting control converges exponentially fast to the one obtained by setting $\dot{\tilde{\beta}} = 0$.
Thus, the uncertain open-loop error system is given by

$$\ddot{\tilde{\beta}} = -\omega_{n0}^2\tilde{\beta} - 2\hat{\rho}\zeta_0\omega_{n0}\dot{\tilde{\beta}} + \hat{\delta}\omega_{n0}^2\tilde{\beta}_r - \Delta_\delta\omega_{n0}^2\left(\tilde{\beta} - \tilde{\beta}_r\right) - \Delta_\rho\left(2\zeta_0\omega_{n0}\dot{\tilde{\beta}}\right) \tag{14}$$

where Δ_ρ, Δ_δ are uncertain parameters defined in (7). The following definition gives a formal description of the robust control problem (RCP) considered in this work.

Definition 4. (Robust control problem) Find a linear feedback law of the form

$$\tilde{\beta}_r = k_p\tilde{\beta} + k_d\dot{\tilde{\beta}}$$

such that the resulting uncertain closed-loop error system from (14) is globally asymptotically stable for all uncertainties Δ_ρ, and Δ_δ.

Next, the RCP above is translated into a more tractable associate optimal control problem (OCP)[67,68] formally stated in the following definition.

Definition 5. (Optimal control problem (OCP)) For given positive real numbers q_1 and q_2, find the control law that minimizes the infinite horizon cost functional

$$\int_0^\infty \left(\begin{bmatrix} \tilde{\beta} \\ \dot{\tilde{\beta}} \end{bmatrix}^\top \begin{bmatrix} q_1 & 0 \\ 0 & q_2 \end{bmatrix} \begin{bmatrix} \tilde{\beta} \\ \dot{\tilde{\beta}} \end{bmatrix} + \frac{1}{2}\tilde{\beta}_r^2(\tau) \right) d\tau \tag{15}$$

subject to the certain dynamic system

$$\begin{bmatrix} \dot{\tilde{\beta}} \\ \ddot{\tilde{\beta}} \end{bmatrix} = \begin{bmatrix} 0 & 1 \\ -\omega_{n0}^2 & -2\hat{\rho}\zeta_0\omega_{n0} \end{bmatrix} \begin{bmatrix} \tilde{\beta} \\ \dot{\tilde{\beta}} \end{bmatrix} + \begin{bmatrix} 0 \\ \hat{\delta}\omega_{n0}^2 \end{bmatrix} \beta_r \tag{16}$$

where q_1, and q_2 are positive weights.

The following Lemma gives the solution to the OCP above.

Lemma 2. The optimal control law is

$$\tilde{\beta}_r^* = -\omega_{n0}^2\left(p_{12}\tilde{\beta} + p_2\dot{\tilde{\beta}}\right) \tag{17}$$

where

$$\begin{aligned} p_{12} &= \frac{1}{\hat{\delta}^2\omega_{n0}^2}\left(\sqrt{2\hat{\delta}^2 q_1 + 1} - 1)\right) \\ p_2 &= \frac{1}{\hat{\delta}^2\omega_{n0}^3}\left(\sqrt{2\hat{\delta}^2\omega_{n0}^2\left(q_2 + p_{12}\right) + 4\hat{\rho}^2\zeta_0^2} - 2\hat{\rho}\zeta_0\right) \end{aligned} \tag{18}$$

Proof. The optimal cost to go

$$V_l(t) = \min \int_t^\infty \left(\begin{bmatrix} \tilde{\beta} \\ \dot{\tilde{\beta}} \end{bmatrix}^\top \begin{bmatrix} q_1 & 0 \\ 0 & q_2 \end{bmatrix} \begin{bmatrix} \tilde{\beta} \\ \dot{\tilde{\beta}} \end{bmatrix} + \frac{1}{2}\tilde{\beta}_r^2 \right) d\tau, \tag{19}$$

satisfies the Hamilton-Jacobi-Bellman equation

$$\min_{\tilde{\beta}_r} \left\{ \begin{bmatrix} \tilde{\beta} \\ \dot{\tilde{\beta}} \end{bmatrix}^\top \begin{bmatrix} q_1 & 0 \\ 0 & q_2 \end{bmatrix} \begin{bmatrix} \tilde{\beta} \\ \dot{\tilde{\beta}} \end{bmatrix} + \frac{1}{2}\tilde{\beta}_r + \begin{bmatrix} \frac{\partial V_l}{\partial \tilde{\beta}} & \frac{\partial V_l}{\partial \dot{\tilde{\beta}}} \end{bmatrix} \begin{bmatrix} \dot{\tilde{\beta}} \\ \ddot{\tilde{\beta}} \end{bmatrix} \right\} = 0. \tag{20}$$

from which the optimal control law is obtained as

$$\tilde{\beta}_r^* = -\begin{bmatrix} \frac{\partial V_l}{\partial \tilde{\beta}} & \frac{\partial V_l}{\partial \dot{\tilde{\beta}}} \end{bmatrix} \begin{bmatrix} 0 \\ \hat{\delta}\omega_{n0}^2 \end{bmatrix} \tag{21}$$

with V_l satisfying

$$\begin{bmatrix} \tilde{\beta} \\ \dot{\tilde{\beta}} \end{bmatrix}^\top \begin{bmatrix} q_1 & 0 \\ 0 & q_2 \end{bmatrix} \begin{bmatrix} \tilde{\beta} \\ \dot{\tilde{\beta}} \end{bmatrix} + \begin{bmatrix} \frac{\partial V_l}{\partial \tilde{\beta}} & \frac{\partial V_l}{\partial \dot{\tilde{\beta}}} \end{bmatrix} \begin{bmatrix} 0 & 1 \\ -\omega_{n0}^2 & -2\hat{\rho}\zeta_0\omega_{n0} \end{bmatrix} \begin{bmatrix} \tilde{\beta} \\ \dot{\tilde{\beta}} \end{bmatrix} - \frac{1}{2}\left(\begin{bmatrix} \frac{\partial V_l}{\partial \tilde{\beta}} & \frac{\partial V_l}{\partial \dot{\tilde{\beta}}} \end{bmatrix} \begin{bmatrix} 0 \\ \hat{\delta}\omega_{n0}^2 \end{bmatrix} \right)^2 = 0 \tag{22}$$

Without loss of generality, let

$$V_l = \frac{1}{2}\begin{bmatrix}\tilde{\beta}\\ \dot{\tilde{\beta}}\end{bmatrix}^\top \begin{bmatrix}p_1 & p_{12}\\ p_{12} & p_2\end{bmatrix}\begin{bmatrix}\tilde{\beta}\\ \dot{\tilde{\beta}}\end{bmatrix} \tag{23}$$

where p_1, p_{12}, and p_2 are the solutions of Algebraic Ricatti Equations (AREs) obtained from (22) and (23) as follows

$$\begin{bmatrix}q_1 & 0\\ 0 & q_2\end{bmatrix} + \frac{1}{2}\begin{bmatrix}0 & 1\\ -\omega_{n0}^2 & -2\hat{\rho}\hat{\zeta}_0\omega_{n0}\end{bmatrix}^\top \begin{bmatrix}p_1 & p_{12}\\ p_{12} & p_2\end{bmatrix} + \frac{1}{2}\begin{bmatrix}p_1 & p_{12}\\ p_{12} & p_2\end{bmatrix}\begin{bmatrix}0 & 1\\ -\omega_{n0}^2 & -2\hat{\rho}\hat{\zeta}_0\omega_{n0}\end{bmatrix}$$
$$-\frac{1}{2}\begin{bmatrix}p_1 & p_{12}\\ p_{12} & p_2\end{bmatrix}\begin{bmatrix}0\\ \hat{\delta}\omega_{n0}^2\end{bmatrix}\begin{bmatrix}0\\ \hat{\delta}\omega_{n0}^2\end{bmatrix}^\top \begin{bmatrix}p_1 & p_{12}\\ p_{12} & p_2\end{bmatrix} = 0,$$

$$\begin{bmatrix} q_1 - \frac{1}{2}\hat{\delta}^2\omega_{n0}^4 p_{12}^2 - \omega_{n0}^2 p_{12} & -\frac{1}{2}\omega_{n0}^2 p_2 + \frac{1}{2}p_1 - \hat{\rho}\zeta_0\omega_{n0}p_{12} - \frac{1}{2}\hat{\delta}^2\omega_{n0}^4 p_2 p_{12}\\ -\frac{1}{2}\omega_{n0}^2 p_2 + \frac{1}{2}p_1 - \hat{\rho}\zeta_0\omega_{n0}p_{12} - \frac{1}{2}\hat{\delta}^2\omega_{n0}^4 p_2 p_{12} & q_2 + p_{12} - 2\hat{\rho}\zeta_0\omega_{n0}p_2 - \frac{1}{2}\hat{\delta}^2\omega_{n0}^4 p_2^2\end{bmatrix} = 0.$$

Then, equating each entry to 0 yields:

$$\begin{aligned}\tfrac{1}{2}\hat{\delta}^2\left(\omega_{n0}^2 p_{12}\right)^2 + \omega_{n0}^2 p_{12} &= q_1\\ \tfrac{1}{2}\hat{\delta}^2\omega_{n0}^4 p_2^2 + 2\hat{\rho}\zeta_0\omega_{n0}p_2 &= q_2 + p_{12}\\ p_1 &= \omega_{n0}^2 p_2 + 2\hat{\rho}\zeta_0\omega_{n0}p_{12} + \hat{\delta}^2\omega_{n0}^4 p_2 p_{12}.\end{aligned} \tag{24}$$

The first two equations give the desired expressions for p_{12} and p_2 in (18). Finally, we show that (18), together with p_1 in the third equation renders V_l a positive definite function. It is clear that $p_{12} > 0$ and $p_2 > 0$. Next,

$$\begin{aligned}p_1 p_2 - p_{12}^2 =& \omega_{n0}^2 p_2^2 + 2\hat{\rho}\zeta_0\omega_{n0}p_{12}p_2 + \hat{\delta}^2\omega_{n0}^4 p_2^2 p_{12} - p_{12}^2\\ =& p_{12}\left(\frac{1}{2}\hat{\delta}^2\omega_{n0}^4 p_2^2 + 2\hat{\rho}\zeta_0\omega_{n0}p_2 - p_{12}\right) + \omega_{n0}^2 p_2^2 + \frac{1}{2}\hat{\delta}^2\omega_{n0}^4 p_2^2 p_{12}\\ =& p_{12}q_2 + \omega_{n0}^2 p_2^2 + \frac{1}{2}\hat{\delta}^2\omega_{n0}^4 p_2^2 p_{12} > 0\end{aligned}$$

□

The connection between the solution to the OCP and the RCP is described in the following theorem.

Theorem 2. If the parameters of the OCP in Definition 5 satisfies the sufficient conditions

$$q_1 > \frac{1}{4\hat{\delta}} \quad \text{and } q_2 > \frac{2\zeta_0^2}{\hat{\delta}^2\omega_{n0}^2}, \tag{25}$$

then the solution of the OCP is also a solution to the RCP in Definition 4. Moreover, the origin of the resulting uncertain closed loop error dynamics is globally exponentially stable, for all values of the uncertain parameters, with the decay rate of at least $\frac{2}{\bar{\lambda}}\min\left\{q_1 - \frac{1}{4\hat{\delta}}, q_2 - \frac{2\zeta_0^2}{\hat{\delta}^2\omega_{n0}^2}\right\}$, where $\bar{\lambda}$ is the maximum eigenvalue of the symmetric positive definite matrix $\begin{bmatrix}p_1 & p_{12}\\ p_{12} & p_2\end{bmatrix}$, where p_1, p_2, p_{12} are the corresponding solutions of the AREs in (24).

Proof. It is sufficient to show that the minimal cost functional V_l is a Lyapunov function for the robust control problem in Definition 4. First, we observe that V_l is positive definite and radially unbounded as $V_l > 0, \tilde{\beta} \neq 0, \tilde{\beta}_r \neq 0$ and $V_l = 0, \tilde{\beta} = 0, \dot{\tilde{\beta}} = 0$ and if $\tilde{\beta}, \dot{\tilde{\beta}} \to \infty$, then $V_l \to \infty$. Next, taking the first time derivative

$$\dot{V}_l = \frac{\partial V_l}{\partial \tilde{\beta}}\dot{\tilde{\beta}} + \frac{\partial V_l}{\partial \dot{\tilde{\beta}}}\ddot{\tilde{\beta}}$$

Substituting (14) yields

$$\dot{V}_l = \frac{\partial V_l}{\partial \tilde{\beta}}\dot{\tilde{\beta}} + \frac{\partial V_l}{\partial \dot{\tilde{\beta}}}\left(-\omega_{n0}^2\tilde{\beta} - 2\hat{\rho}\zeta_0\omega_{n0} + \hat{\delta}\omega_{n0}^2\tilde{\beta}_r\right) + \frac{\partial V_l}{\partial \dot{\tilde{\beta}}}\left(-\Delta_\delta\omega_{n0}^2\tilde{\beta} - 2\Delta_\rho\zeta_0\omega_{n0}\dot{\tilde{\beta}} + \Delta_\delta\omega_{n0}^2\tilde{\beta}_r\right).$$

Then, inserting the optimal control law (21) in Lemma. 2 leads to

$$\dot{V}_l = -\omega_{n0}^2\frac{\partial V_l}{\partial \dot{\tilde{\beta}}}\tilde{\beta} + \left(\frac{\partial V_l}{\partial \tilde{\beta}} - 2\hat{\rho}\zeta_0\omega_{n0}\frac{\partial V_l}{\partial \dot{\tilde{\beta}}}\right)\dot{\tilde{\beta}} - \hat{\delta}^2\omega_{n0}^4\left(\frac{\partial V_l}{\partial \dot{\tilde{\beta}}}\right)^2 + \frac{\partial V_l}{\partial \dot{\tilde{\beta}}}\left(-\Delta_\delta\omega_{n0}^2\tilde{\beta} - 2\Delta_\rho\zeta_0\omega_{n0}\dot{\tilde{\beta}}\right) - \Delta_\delta\hat{\delta}\omega_{n0}^4\left(\frac{\partial V_l}{\partial \dot{\tilde{\beta}}}\right)^2.$$

Using (22) yields

$$\begin{aligned}\dot{V}_l &= -q_1\tilde{\beta}^2 - q_2\dot{\tilde{\beta}}^2 - \frac{1}{2}\hat{\delta}^2\omega_{n0}^4\left(\frac{\partial V_l}{\partial\dot{\tilde{\beta}}}\right)^2 - \Delta_\delta\omega_{n0}^2\frac{\partial V_l}{\partial\dot{\tilde{\beta}}}\tilde{\beta} - 2\Delta_\rho\zeta_0\omega_{n0}\frac{\partial V_l}{\partial\dot{\tilde{\beta}}}\dot{\tilde{\beta}} - \Delta_\delta\hat{\delta}\omega_{n0}^4\left(\frac{\partial V_l}{\partial\dot{\tilde{\beta}}}\right)^2\\ &= -q_1\tilde{\beta}^2 - q_2\dot{\tilde{\beta}}^2 - \Delta_\delta\omega_{n0}^2\left(\frac{\partial V_l}{\partial\dot{\tilde{\beta}}}\tilde{\beta} + \hat{\delta}\omega_{n0}^2\left(\frac{\partial V_l}{\partial\dot{\tilde{\beta}}}\right)^2\right) - 2\omega_{n0}^2\left(\frac{\zeta_0}{\omega_{n0}}\Delta_\rho\frac{\partial V_l}{\partial\dot{\tilde{\beta}}}\dot{\tilde{\beta}} + \frac{1}{4}\hat{\delta}^2\omega_{n0}^2\left(\frac{\partial V_l}{\partial\dot{\tilde{\beta}}}\right)^2\right)\\ &= -q_1\tilde{\beta}^2 - q_2\dot{\tilde{\beta}}^2 - \Delta_\delta\omega_{n0}^2\left(\left(\frac{\tilde{\beta}}{2\sqrt{\hat{\delta}}\omega_{n0}} + \sqrt{\hat{\delta}}\omega_{n0}\frac{\partial V_l}{\partial\dot{\tilde{\beta}}}\right)^2 - \frac{\tilde{\beta}^2}{4\hat{\delta}\omega_{n0}^2}\right) - 2\omega_{n0}^2\left(\left(\frac{\zeta_0}{\hat{\delta}\omega_{n0}^2}\Delta_\rho\dot{\tilde{\beta}} + \frac{1}{2}\hat{\delta}\omega_{n0}\frac{\partial V_l}{\partial\dot{\tilde{\beta}}}\right)^2 - \frac{\zeta_0^2}{\hat{\delta}^2\omega_{n0}^4}\Delta_\rho^2\dot{\tilde{\beta}}^2\right)\end{aligned}$$

Thus

$$\begin{aligned}\dot{V}_l &\le -\left(q_1 - \frac{1}{4\hat{\delta}}\right)\tilde{\beta}^2 - \left(q_2 - \frac{2\zeta_0^2}{\hat{\delta}^2\omega_{n0}^2}\right)\dot{\tilde{\beta}}^2\\ &\le -k_\delta\tilde{\beta}^2 - k_\rho\dot{\tilde{\beta}}^2.\end{aligned} \tag{26}$$

where $k_\delta \triangleq q_1 - \dfrac{1}{4\hat{\delta}} > 0$, and $k_\rho \triangleq q_2 - \dfrac{2\zeta_0^2}{\hat{\delta}^2\omega_{n0}^2} > 0$.

Next, From Lemma. 2, V_l is positive definite. Thus, it satisfies

$$\frac{1}{2}\bar{\lambda}\left\|\begin{bmatrix}\tilde{\beta}\\ \dot{\tilde{\beta}}\end{bmatrix}\right\|^2 \ge V_l. \tag{27}$$

From (26), it follows that

$$\dot{V}_l \le -\min\left\{k_\delta, k_\rho\right\}\left\|\begin{bmatrix}\tilde{\beta}\\ \dot{\tilde{\beta}}\end{bmatrix}\right\|^2.$$

Using (27) yields

$$\dot{V}_l \le -2\frac{\min\left\{k_\delta, k_\rho\right\}}{\bar{\lambda}}V_l.$$

Using the comparison lemma[69] results in

$$V_l(t) \le V_l(0)\exp\left(-2\frac{\min\left\{k_\delta, k_\rho\right\}}{\bar{\lambda}}t\right).$$

□

5 | NUMERICAL SIMULATION

5.1 | Numerical design parameters

The high-level control design parameters are chosen such that the sufficient condition in (11) is satisfied. First, we should find the lower and upper bound parameters c_b, and c_v. We know that the range of the wind speed in the full-load region is $11.4\ \mathsf{m/s} \le v \le 25\ \mathsf{m/s}$ and the rated rotor speed is $\omega_0 = 1.267\ \mathsf{rad/sec}$. Next, we obtain the parameters m_1, m_2, and m_3 in (4) by solving an optimization problem constrained by (4) at the steady state condition at the operating point $\omega_{n0} = 11.11\ \mathsf{rad/sec}$, $\zeta_0 = 0.6$, and $\beta_0 = 19.94\ \mathsf{deg}$. This gives $m_1 = 5.4184$, $m_2 = 0.0682$, $m_3 = 0.029$. Consequently, the lower and upper bound parameters are obtained as $c_b = 0.001, c_v = 2$.

Three different values of γ (0.85, 0.9 and 1) are used to evaluate the performance of the designed high-level controller and to asses how the values of γ influence the robustness and control authority. The control gain k is fixed at $k = 2500$ and α is calculated for each γ such that the sufficient condition in (11) holds. Moreover, $\phi_0 = 1192.8\ \mathsf{deg}^2$, $\bar{\beta} = 90\ \mathsf{deg}$, $\bar{\phi} = 24300\ \mathsf{deg}^2$ are used for the sat function.

In the low-level loop, we consider high-air content fault changing the natural frequency and the damping ratio of the closed-loop pitch actuator model to $\zeta_a = 0.9$, and $\omega_{na} = 3.42\ \mathsf{rad/sec}$[61]. Consequently, we set $\hat{\delta} = 0.1\ \mathsf{rad}^2/\mathsf{sec}^2$, then the sufficient

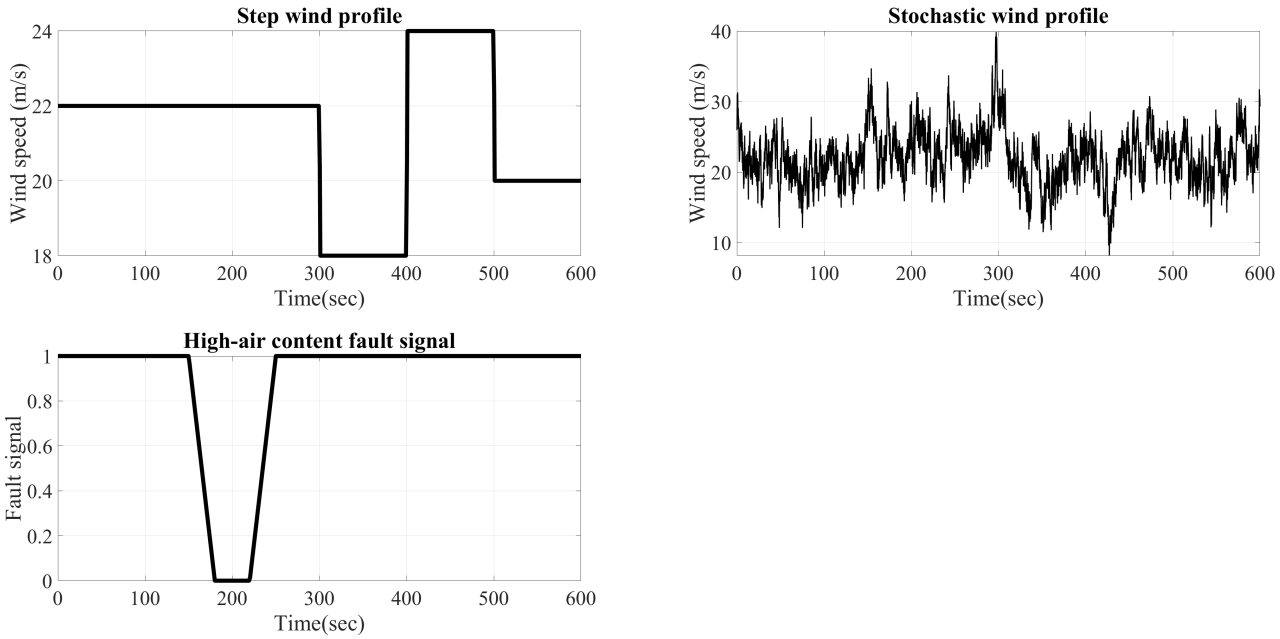

FIGURE 4 Input profiles

condition in (25) is satisfied by setting $q_1 > 2.5$, $q_2 > 0.6$. To obtain a good transient performance in response to the faults, we choose sufficiently large values $q_1 = 25$, and $q_2 = 1$.

5.1.1 | Simulation study

The proposed approach is implemented on a 5-MW-3-bladed-variable-pitch wind turbine using the FAST simulator. The results are compared with an adaptive ISMC[24], and a well-tuned PI-gain-scheduling controller developed by NREL[58]. Two scenarios have been used to testify the controller. First, we consider a step-wind profile at different operating points. Then, an stochastic wind profile is applied. Both scenarios include pitch actuator faults. Also, three different γ–s are used for the developed controller to study its robustness.

Fig. 4 shows input signals, including a step wind profile, an stochastic wind profile, and a fault signal. The stochastic wind profile generated by the TurbSim software[70]with 13×13 vertical and horizontal grid of IEC class A Kimal spectrum turbulence with the mean speed of $22m/s$, and the turbulence intensity of $TI = 19\%$ (20 in the software) with the sample time of 0.05s, and it shows that the generated stochastic wind profile covers the full-load region completely. In this paper, we consider the high-air content actuator fault, which is linearly activated between 150sec-180sec, then fully activated between 180sec-220sec, and linearly vanished between 220sec-250sec. Note that the fault is an active-low signal. Fig. 5 shows that the adaptive ISMC, and especially the PI-gain-scheduling controller have huge oscillations when the wind speed changes, which causes negative spikes in the electrical power for the latter. It shows that the generator torque for the PI-gain-scheduling controller goes to saturation several times. Also, note that the developed controller with the lowest amount of gamma ($\gamma = 0.85$) has weaker transient response in comparison with the higher ones, but its performance is still better than both the PI-gain-scheduling controller and the adaptive ISMC. Also, the control authority shows that the proposed controller makes less control effort, while its performance is significantly better than the other two controllers. Fig. 6 shows the rotor speed and the pitch angle under the incipient high-air content fault, which mostly affects the PI-gain-scheduling controller and the adaptive ISMC. Notice that all controllers have small oscillations in their steady state response due to the noise in the rotor speed. To testify the controller in a more realistic situation, we use the stochastic wind profile shown in Fig. 4 along with the same pitch actuator fault's scenario. Fig. 7 shows that the PI-gain-scheduling controller has much more fluctuations in its rotor speed response compared with the adaptive ISMC. In addition, the adaptive ISMC has big oscillations between 300s-400s, when the wind speed suddenly drops. Note that increasing the gamma reduces the fluctuations for the developed controller. Also, it shows that the generator torque has been affected by the oscillations in the rotor speed, and thereby the PI-gain-scheduling controller goes to saturation multiple times with negative spikes in the electrical power. Note that because the high-air content is an incipient fault, its effect is not that distinguishable

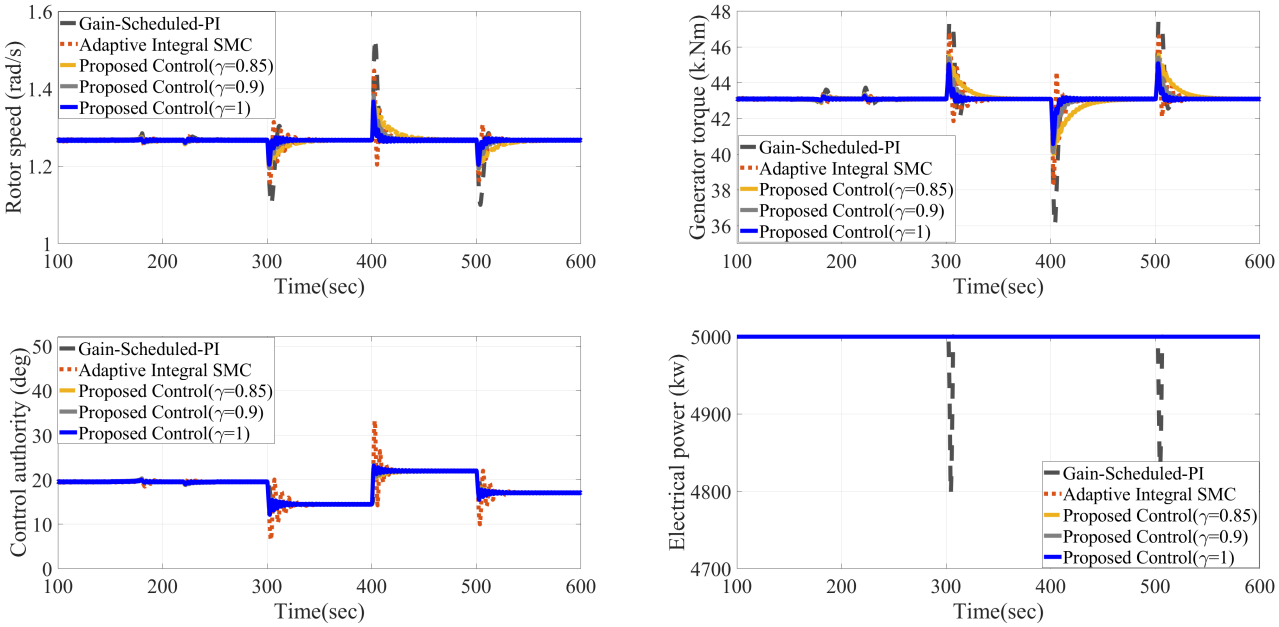

FIGURE 5 Rotor speed, control input, generator torque and electrical power subject to the step wind profile

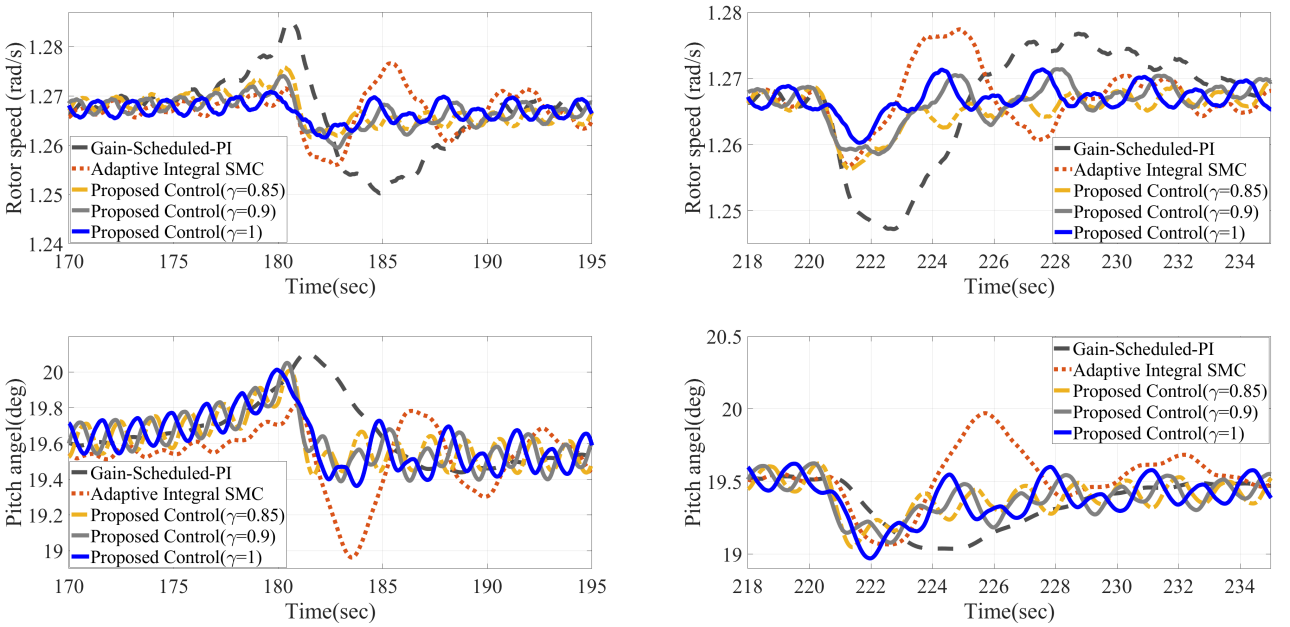

FIGURE 6 Rotor speed and the pitch angle subject to the high-air content actuator fault and the step wind signal

under the stochastic wind signal. Table. 1 shows the root mean square (rms) of the error and the high-level control authority for the adaptive ISMC, and the proposed controller with different gammas as a percentage of the PI-gain-scheduling controller as the baseline control. It shows that the rms of the error in the rotor speed has been reduced to 57% using the adaptive ISMC, and 27% using the developed controller (with the biggest gamma) under the step wind signal. It also shows a reduction up to 48% for the adaptive ISMC and to 27% for the proposed controller under the stochastic wind profile. However, the results show that the rms of the control authority is almost the same. Moreover, it shows that the developed controller with the biggest gamma has the biggest reduction in the rms of the error.

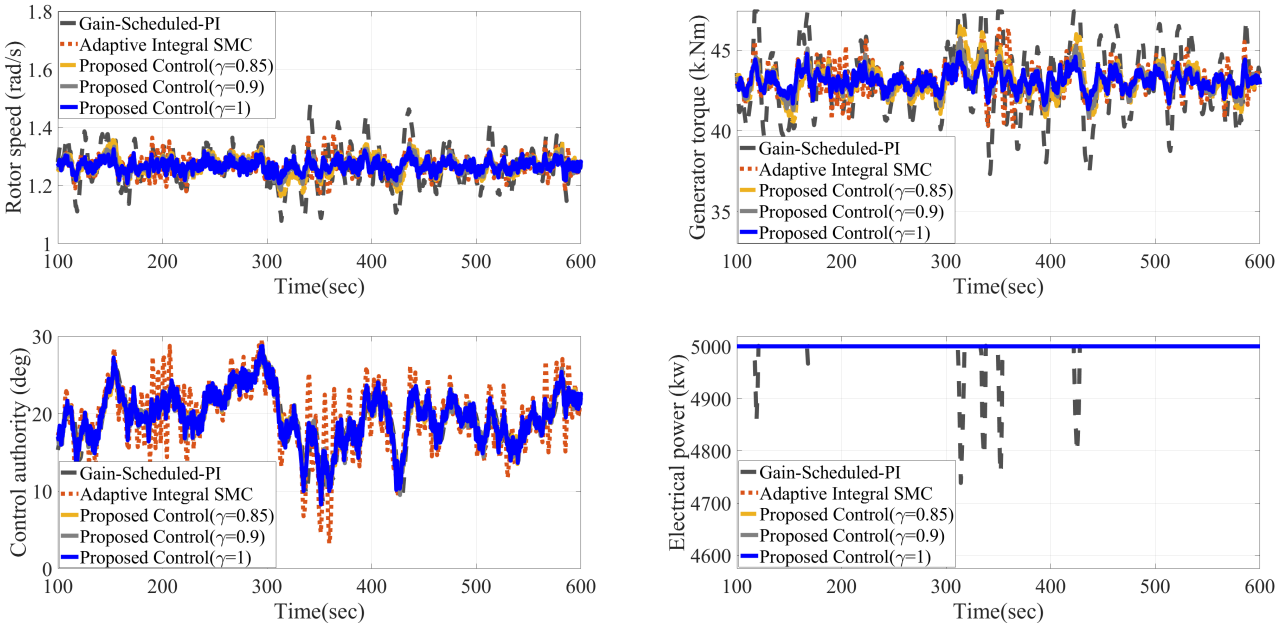

FIGURE 7 Rotor speed, control input, generator torque and electrical power subject to the stochastic wind signal

Wind type	Step		Stochastic	
Rms	Error	Control authority	Error	Control authority
Gain-Scheduled PI Controller	100%	100%	100%	100%
Adaptive ISMC	57%	100.1%	48%	101%
Proposed Controller ($\gamma = 0.85$)	55%	99.9%	44%	99.9%
Proposed Controller($\gamma = 0.9$)	37%	100%	34%	100.1%
Proposed Controller($\gamma = 1$)	27%	100%	27%	100.2%

TABLE 1 Rms of errors and control inputs related to the step wind signal

6 | CONCLUSION

A two-layered control architecture was designed to robustly regulate the output of variable-pitch wind turbine subject to wind variation and pitch actuator faults. The high-level control is a robust control using the concept of dissipativity to accommodate system nonlinearity while mitigating the effect of wind disturbance on the rotor dynamics. The low-level design uses optimal control to robustly mitigate the actuator faults while tracking the high-level commands with guaranteed performance. The simulation results show that, although the controller is simple and easy to implement, compared to results in literature, it has a better performance in dealing with model variation, the actuator fault, and wind disturbance.

References

1. Wu B, Lang Y, Zargari N, Kouro S. *Power conversion and control of wind energy systems*. 76. John Wiley & Sons . 2011.
2. Manwell JF, McGowan JG, Rogers AL. *Wind energy explained: theory, design and application*. John Wiley & Sons . 2010.
3. Heier S. *Grid integration of wind energy: onshore and offshore conversion systems*. John Wiley & Sons . 2014.
4. Ackermann T. *Wind power in power systems*. John Wiley & Sons . 2005.

5. Billinton R, Bai G. Generating capacity adequacy associated with wind energy. *IEEE transactions on energy conversion* 2004; 19(3): 641–646.

6. Novak P, Ekelund T, Jovik I, Schmidtbauer B. Modeling and control of variable-speed wind-turbine drive-system dynamics. *IEEE Control Systems Magazine* 1995; 15(4): 28–38.

7. Pao LY, Johnson KE. Control of wind turbines. *IEEE Control systems magazine* 2011; 31(2): 44–62.

8. Bianchi F. H., Battista, R., Mantz. *Wind turbine control systems–Principles, modeling, and gain scheduling design, Springer-Verlag, Berlin* 2007.

9. Meng F, Wenske J, Gambier A. Wind turbine loads reduction using feedforward feedback collective pitch control based on the estimated effective wind speed. In: IEEE. ; 2016: 2289–2294.

10. Sarkar S, Fitzgerald B, Basu B. Individual blade pitch control of floating offshore wind turbines for load mitigation and power regulation. *IEEE Transactions on Control Systems Technology* 2020; 29(1): 305–315.

11. Abrazeh S, Parvaresh A, Mohseni SR, Zeitouni MJ, Gheisarnejad M, Khooban MH. Nonsingular Terminal Sliding Mode Control With Ultra-Local Model and Single Input Interval Type-2 Fuzzy Logic Control for Pitch Control of Wind Turbines. *IEEE/CAA Journal of Automatica Sinica* 2021; 8(3): 690–700.

12. Palejiya D, Chen D. Performance improvements of switching control for wind turbines. *IEEE Transactions on Sustainable Energy* 2015; 7(2): 526–534.

13. Kalbat A. Linear quadratic gaussian (lqg) control of wind turbines. In: IEEE. ; 2013: 1–5.

14. Zhang Y, Cheng M, Chen Z. Load mitigation of unbalanced wind turbines using PI-R individual pitch control. *IET Renewable Power Generation* 2014; 9(3): 262–271.

15. Imran RM, Hussain DA, Soltani M. DAC with LQR control design for pitch regulated variable speed wind turbine. In: IEEE. ; 2014: 1–6.

16. Selvam K, Kanev S, Wingerden vJW, Engelen vT, Verhaegen M. Feedback–feedforward individual pitch control for wind turbine load reduction. *International Journal of Robust and Nonlinear Control: IFAC-Affiliated Journal* 2009; 19(1): 72–91.

17. Jafarnejadsani H, Pieper J. Gain-Scheduled ℓ_1 -Optimal Control of Variable-Speed-Variable-Pitch Wind Turbines. *IEEE Transactions on Control Systems Technology* 2015; 23(1): 372-379. doi: 10.1109/TCST.2014.2320675

18. Van TL, Nguyen TH, Lee DC. Advanced pitch angle control based on fuzzy logic for variable-speed wind turbine systems. *IEEE Transactions on Energy Conversion* 2015; 30(2): 578–587.

19. Tong X, Zhao X. Power Generation Control of a Monopile Hydrostatic Wind Turbine Using an $\mathcal{H}_\infty$ Loop-Shaping Torque Controller and an LPV Pitch Controller. *IEEE Transactions on control systems technology* 2017; 26(6): 2165–2172.

20. Jafarnejadsani H, Pieper J. Gain-Scheduled l_1-Optimal Control of Variable-Speed-Variable-Pitch Wind Turbines. *IEEE Transactions on Control Systems Technology* 2014; 23(1): 372–379.

21. Wang CS, Chiang MH. A novel pitch control system of a large wind turbine using two-degree-of-freedom motion control with feedback linearization control. *Energies* 2016; 9(10): 791.

22. Shang L, Hu J. Sliding-mode-based direct power control of grid-connected wind-turbine-driven doubly fed induction generators under unbalanced grid voltage conditions. *IEEE Transactions on Energy Conversion* 2012; 27(2): 362–373.

23. Azizi A, Nourisola H, Shoja-Majidabad S. Fault tolerant control of wind turbines with an adaptive output feedback sliding mode controller. *Renewable energy* 2019; 135: 55–65.

24. Ameli S, Morshed MJ, Fekih A. Adaptive Integral Sliding Mode Design for the Pitch Control of a Variable Speed Wind Turbine. In: IEEE. ; 2019: 290–295.

25. Odgaard PF, Stoustrup J, Kinnaert M. Fault tolerant control of wind turbines–a benchmark model. *IFAC Proceedings Volumes* 2009; 42(8): 155–160.

26. Odgaard PF, Stoustrup J, Kinnaert M. Fault-tolerant control of wind turbines: A benchmark model. *IEEE Transactions on control systems Technology* 2013; 21(4): 1168–1182.

27. Sloth C, Esbensen T, Stoustrup J. Robust and fault-tolerant linear parameter-varying control of wind turbines. *Mechatronics* 2011; 21(4): 645–659.

28. Luo N, Vidal Y, Acho L. *Wind turbine control and monitoring*. Springer . 2014.

29. Simani S, Castaldi P. Active actuator fault-tolerant control of a wind turbine benchmark model. *International Journal of Robust and Nonlinear Control* 2014; 24(8-9): 1283–1303.

30. Ameli S, Anubi OM. Hierarchical Robust Adaptive Control for Wind Turbines with Actuator Fault. *ASME Letters in Dynamic Systems and Control* 2022.

31. Stefanovski JD. Fault tolerant control of descriptor systems with disturbances. *IEEE Transactions on Automatic Control* 2018; 64(3): 976–988.

32. Stefanovski JD. Passive fault tolerant perfect tracking with additive faults. *Automatica* 2018; 87: 432–436.

33. Xiong J, Chang XH, Park JH, Li ZM. Nonfragile fault-tolerant control of suspension systems subject to input quantization and actuator fault. *International Journal of Robust and Nonlinear Control* 2020; 30(16): 6720–6743.

34. Li J, Wang S. Dual multivariable model-free adaptive individual pitch control for load reduction in wind turbines with actuator faults. *Renewable Energy* 2021; 174: 293–304.

35. Ameli S, Anubi OM. Robust Control for a Class of Nonlinearly Coupled Hierarchical Systems with Actuator Faults. *IFAC-PapersOnLine* 2021; 54(20): 540–546.

36. Huang C, Naghdy F, Du H. Delta operator-based fault estimation and fault-tolerant model predictive control for steer-by-wire systems. *IEEE Transactions on Control Systems Technology* 2017; 26(5): 1810–1817.

37. Jain T, Yamé JJ. Fault-Tolerant Economic Model Predictive Control for Wind Turbines. *IEEE Transactions on Sustainable Energy* 2018; 10(4): 1696–1704.

38. Witczak P, Pazera M, Patan K, Witczak M. Constrained actuator fault tolerant control with the application to a wind turbine. *IFAC-PapersOnLine* 2018; 51(24): 1157–1163.

39. Badihi H, Zhang Y, Pillay P, Rakheja S. Fault-tolerant individual pitch control for load mitigation in wind turbines with actuator faults. *IEEE Transactions on Industrial Electronics* 2020; 68(1): 532–543.

40. Kühne P, Pöschke F, Schulte H. Fault estimation and fault-tolerant control of the FAST NREL 5-MW reference wind turbine using a proportional multi-integral observer. *International Journal of Adaptive Control and Signal Processing* 2018; 32(4): 568–585.

41. Mazare M, Taghizadeh M, Ghaf-Ghanbari P. Fault tolerant control of wind turbines with simultaneous actuator and sensor faults using adaptive time delay control. *Renewable Energy* 2021; 174: 86–101.

42. Liu Y, Patton RJ, Shi S. Asymmetrical Load Mitigation of Wind Turbine Pitch Actuator Faults using Unknown Input-based Fault-tolerant Control. *IFAC-PapersOnLine* 2020; 53(2): 699–704.

43. Mazare M, Taghizadeh M, Ghaf-Ghanbari P. Pitch actuator fault-tolerant control of wind turbines based on time delay control and disturbance observer. *Ocean Engineering* 2021; 238: 109724.

44. Odgaard PF, Stoustrup J. A benchmark evaluation of fault tolerant wind turbine control concepts. *IEEE Transactions on Control Systems Technology* 2014; 23(3): 1221–1228.

45. Qi K, De-hui S, Zheng-xi L, Shu-juan Q, Yan-jiao H, Yun-tao S. H_∞ fault tolerant control of wind turbine system with actuator faults. *IFAC Proceedings Volumes* 2014; 47(3): 5838–5843.

46. Colombo L, Corradini M, Ippoliti G, Orlando G. Pitch angle control of a wind turbine operating above the rated wind speed: A sliding mode control approach. *ISA transactions* 2020; 96: 95–102.

47. Sørensen KL, Galeazzi R, Odgaard PF, Niemann H, Poulsen NK. Adaptive passivity based individual pitch control for wind turbines in the full load region. In: IEEE. ; 2014: 554–559.

48. Yarmohammadi MJ, Sadeghzadeh A, Taghizadeh M. Gain-scheduled control of wind turbine exploiting inexact wind speed measurement for full operating range. *Renewable Energy* 2020; 149: 890–901.

49. Wang X, Zhou J, Qin B, Luo Y, Hu C, Pang J. Individual Pitch Control of Wind Turbines Based on SVM Load Estimation and LIDAR Measurement. *IEEE Access* 2021; 9: 143913–143921.

50. Xiao S, Geng H, Yang G. Non-linear pitch control of wind turbines for tower load reduction. *IET Renewable Power Generation* 2014; 8(7): 786–794.

51. Baiomy N, Kikuuwe R. An amplitude-and rate-saturated collective pitch controller for wind turbine systems. *Renewable Energy* 2020.

52. Bao J, Wang M, Yue H, Leithead W. Pseudo-lidar data analysis and feed-forward wind turbine control design. *IFAC-PapersOnLine* 2015; 48(8): 483–488.

53. Jiao X, Yang Q, Xu B. Hybrid Intelligent Feedforward-feedback Pitch Control for VSWT with Predicted Wind Speed. *IEEE Transactions on Energy Conversion* 2021.

54. Wei X, Dong L, Zhang H, Hu X, Han J. Adaptive disturbance observer-based control for stochastic systems with multiple heterogeneous disturbances. *International Journal of Robust and Nonlinear Control* 2019; 29(16): 5533–5549.

55. Ren Y, Li L, Brindley J, Jiang L. Nonlinear PI control for variable pitch wind turbine. *Control Engineering Practice* 2016; 50: 84–94.

56. Schaft v. dAJ, Van Der Schaft A. *L2-gain and passivity techniques in nonlinear control*. 2. Springer . 2000.

57. Anubi OM. *Variable stiffness suspension system*. University of Florida . 2013.

58. Jonkman J, Butterfield S, Musial W, Scott G. Definition of a 5-MW reference wind turbine for offshore system development. tech. rep., National Renewable Energy Lab.(NREL), Golden, CO (United States); : 2009.

59. Bianchi FD, De Battista H, Mantz RJ. *Wind turbine control systems: principles, modelling and gain scheduling design*. Springer Science & Business Media . 2006.

60. Wasynczuk O, Man D, Sullivan J. Dynamic behavior of a class of wind turbine generators during random wind fluctuations. *IEEE Transactions on power apparatus and systems* 1981(6): 2837–2845.

61. Odgaard PF, Johnson KE. Wind turbine fault detection and fault tolerant control-an enhanced benchmark challenge. In: IEEE. ; 2013: 4447–4452.

62. Rudin W, others . *Principles of mathematical analysis*. 3. McGraw-hill New York . 1964.

63. Benlahrache MA, Laib K, Othman S, Sheibat-Othman N. Fault Tolerant Control of Wind Turbine Using Robust Model Predictive Min-Max approach. *IFAC-PapersOnLine* 2017; 50(1): 9902–9907.

64. Rezaei V, Johnson KE. Robust fault tolerant pitch control of wind turbines. In: IEEE. ; 2013: 391–396.

65. Anubi OM, Crane C. A new semiactive variable stiffness suspension system using combined skyhook and nonlinear energy sink-based controllers. *IEEE Transactions on Control Systems Technology* 2014; 23(3): 937–947.

66. Anubi OM, Crane III CD. Roll stabilisation of road vehicles using a variable stiffness suspension system. *Vehicle system dynamics* 2013; 51(12): 1894–1917.

67. Lin F. An optimal control approach to robust control design. *International journal of control* 2000; 73(3): 177–186.

68. Lin F, Brandt RD, Sun J. Robust control of nonlinear systems: Compensating for uncertainty. *International Journal of Control* 1992; 56(6): 1453–1459.

69. Hassan K. Khalil, nonlinear systems. *Prentice-Hall, Inc., New Jersey* 1996.

70. Jonkman BJ. TurbSim user's guide: Version 1.50. tech. rep., National Renewable Energy Lab.(NREL), Golden, CO (United States); : 2009.

How to cite this article: Ameli S., Anubi O.M., Hierarchical robust control for variable-pitch wind turbine with actuator faults, *Int J Robust Nonlinear Control.*, *2020;1–18.*